Multi-Sensor Full-Polarimetric SAR Automatic Target Recognition Using Pseudo-Zernike Moments

Carmine Clemente*, Luca Pallotta†, Ian Proudler ‡, Antonio De Maio†,
John J. Soraghan*, and Alfonso Farina§
*University of Strathclyde, CESIP, EEE, 204, George Street, G1 1XW, Glasgow, UK
E-mail: carmine.clemente@strath.ac.uk, j.soraghan@strath.ac.uk
†Università degli Studi di Napoli "Federico II", DIETI, via Claudio 21, I-80125 Napoli, Italy
E-mail: luca.pallotta@unina.it, ademaio@unina.it
‡ School of Electronic, Electrical and Systems Engineering, Loughborough University, Leicestershire, UK
E-mail: i.k.proudler@lboro.ac.uk
§Selex ES, via Tiburtina Km.12.4, I-00131 Roma, Italy
E-mail: alfonso.farina@selex-es.com

***Abstract*—In the modern battlefield scenario multiple sources of information may be exploited to mitigate uncertainty. Polarization and spatial diversity can provide useful information for specific and critical tasks such as the Automatic Target Recognition (ATR). In this paper the use of pseudo-Zernike moments applied to the full-polarimetric Gotcha dataset is presented. Specifically improved single platform ATR performance is demonstrated through the use of multiple observations.**

I. Introduction

In the modern battlefield scenarios the availability of multiple sources of information, such as spatial, temporal or other diversities, allows improvements in sensor performance and capabilities. In particular, modern radar scenario involves different diversities, some provided by the sensor position in the space-time plane: spatial diversity given by multiple platforms observing from different positions and temporal diversity provided by multiple passes over the same area from the same platform, and their combinations; and others given by different sensor characteristics: frequency, waveform and polarization diversity. Of particular interest is the combination of these two categories of diversities that can be described as a Distributed Multiple-Input Multiple-Output Radar Sensor Network (DMRS).

In our work we investigate the possibility of exploiting this information for improving the performance compared to that possible from a classic Single-Input Single-Output system. Other important aspects include the ability of achieving high performance with low cost algorithms and the capability to summarize the discriminating information thereby reducing the communication overload between sensors.

A particular application is Automatic Target Recognition (ATR) [1], [2], [3] and its lower level tasks (identification, characterization and fingerprinting) from Synthetic Aperture Radar (SAR) data. Moreover, the way in which targets scatter signals of different polarizations also contains information that can be exploited in target recognition, so the use of full-polarization SAR data can lead to improved ATR performance and for this reason is also of particular interest.

In this paper an algorithm for ATR, with target identification capabilities, from multiple spatially separated full-polarimetric SAR data is presented. The algorithm exploits full-polarimetric information and, at low computational cost, extracts reliable and easy-to-share discriminating features based on the pseudo-Zernike moments. The proposed algorithm is tested with the Gotcha dataset [4] that contains multiple observations of commercial vehicles.

The remainder of the paper is organised as follow. In Section II, the novel algorithm to extract the features from a full polarimetric SAR observation is introduced together with the decision fusion framework for the case of multiple passes. Section III introduces the Gotcha dataset and present the results obtained with different data training set for the case of 1, 2 and 3 sensors sharing the individual classification outputs. Section IV concludes the paper.

II. Features Extraction Exploiting Pseudo-Zernike Moments

In this section, a novel feature for full polarimetric ATR is introduced. The approach is based on the use of pseudo-Zernike moments [5], to obtain reliable feature vectors with relatively small dimension and low computational complexity. The use of pseudo-Zernike moments was introduced in the radar literature for the ATR applied to micro-Doppler signatures [6]. The novel feature benefits from specific properties of the pseudo-Zernike moments such as invariance with respect to translation and rotation and in addition scale invariance can be included if required by the specific applications.

In the following subsections the background theory defining the pseudo-Zernike moments is introduced, followed by the novel feature extraction algorithm and the decision fusion framework.

A. Pseudo-Zernike Moments

Let $f(x,y)$ be a non-negative real image. The complex pseudo-Zernike moments can be computed as [5]

$$\psi_{n,l} = \frac{n+1}{\pi} \int_0^{2\pi} \int_0^1 W^*_{n,l}\left(\rho\cos\theta, \rho\sin\theta, \rho\right) \cdot f(\rho\cos\theta, \rho\sin\theta)\rho d\rho d\theta, \tag{1}$$

where the symbol $(\cdot)^*$ indicates the complex conjugate operator and $W_{n,l}$ are the pseudo-Zernike polynomials. The latter are a set of orthogonal functions that can be written in the form

$$\begin{aligned} W_{n,l}\left(x,y,\rho\right) &= W_{n,l}\left(\rho\cos\theta,\rho\sin\theta,\rho\right) \\ &= S_{n,l}\left(\rho\right)e^{jl\theta}, \end{aligned} \tag{2}$$

with $j = \sqrt{-1}$, $x = \rho\cos\theta$, $y = \rho\sin\theta$, l an integer, and $S_{n,l}(\rho)$ a polynomial (called a radial polynomial) in ρ of degree n such that $n \geq |l|$. Notice that the modulus of (2) is rotational invariant [5]. Moreover, these functions form a complete basis and satisfy, on the unit disc (i.e. for $x^2 + y^2 \leq 1$), the orthogonality relation [5]

$$\begin{aligned} \iint_{x^2+y^2\leq 1} W^*_{n,l}\left(x,y,x^2+y^2\right)W_{m,k}\left(x,y,x^2+y^2\right)\cdot \\ dx\,dy = \frac{\pi}{n+1}\delta_{mn}\delta_{kl}, \end{aligned} \tag{3}$$

where δ_{mn} is the Kronecker delta function, i.e. $\delta_{mn} = 1$ if $m = n$, and 0 otherwise. Finally, as given in [5], the radial polynomials, $S_{n,l}(\rho)$, can be computed through their explicit expressions

$$S_{n,l}(\rho) = \sum_{k=0}^{n-|l|} \frac{\rho^{n-k}(-1)^k\,(2n+1-k)!}{k!\,(n+|l|+1-k)!\,(n-|l|-k)!}. \tag{4}$$

Notice that, for a given n the number of linearly independent pseudo-Zernike polynomials is $(n+1)^2$. Moreover, as previously stated an important characteristic of the pseudo-Zernike moments is the simple rotational transformation property due to (2); indeed, the moment requires only a phase factor for the rotation [5].

B. Feature Extraction Algorithm

The feature extraction algorithm is summarized in the block diagram shown in Figure 1, while a detailed explanation of the processing steps is described below.

The complex valued image for each polarization from the j-th sensor is defined as $\mathbf{X}_j(x,y,i) \in \mathbb{C}^{B\times Z\times 4}$ with x and y representing the range and cross-range pixel, respectively, of the $B \times Z$ sub-image containing the target and i the index of the i-th component of the vector $\mathbf{p} = [HH, VV, HV, VH]$ identifying the transmitter/receiver polarization.

The feature extraction algorithm begins with the generation of the full polarimetric magnitude image of the target area

$$\boldsymbol{\Omega}_j(x,y) = \sum_{i=1}^{4} |\mathbf{X}_j(x,y,i)|. \tag{5}$$

As the value of $\boldsymbol{\Omega}_j(x,y)$ can cover a very large range of values, its logarithm is used instead

$$\tilde{\boldsymbol{\Omega}}_j(x,y) = \log_{10}(\boldsymbol{\Omega}_j(x,y)). \tag{6}$$

In order to obtain features that are independent of different intensity levels, due to different observation angles and channel propagation properties, a normalization of $\tilde{\boldsymbol{\Omega}}_j$ is required to restrict its magnitude to the interval $[0,1]$

$$\begin{aligned} \overline{\boldsymbol{\Omega}}_j(x,y) &= \tilde{\boldsymbol{\Omega}}_j(x,y) - \min[\tilde{\boldsymbol{\Omega}}_j(x,y)], \\ \hat{\boldsymbol{\Omega}}_j(x,y) &= \overline{\boldsymbol{\Omega}}_j(x,y)/\max(\overline{\boldsymbol{\Omega}}_j(x,y)). \end{aligned} \tag{7}$$

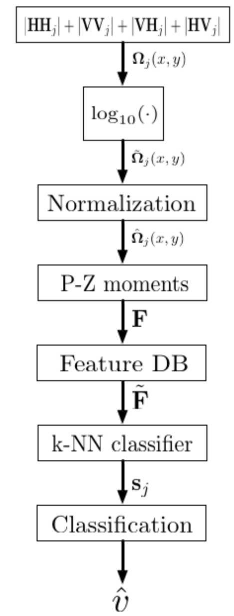

Fig. 1. Block diagram of the proposed feature extraction and classification algorithm.

Next step of the algorithm (Fig. 1) is the projection of $\hat{\boldsymbol{\Omega}}_j(x,y)$ onto a basis of pseudo-Zernike polynomials. The polynomials can be pre-computed through (4) since it depends on the sub-image size $B \times Z$ only (due to the dependencies of (4) only on ρ), and therefore may be used to populate a look up table. As the pseudo-Zernike polynomials are defined on the unit disc, the support of the image $\hat{\boldsymbol{\Omega}}_j(x,y)$ is scaled, before the moments are computed, to avoid information loss. Applying (1) to $\hat{\boldsymbol{\Omega}}_j(x,y)$, the pseudo-Zernike expansion is obtained as

$$\begin{aligned} \psi_{n,l} = \frac{n+1}{\pi}\int_0^{2\pi}\int_0^1 W^*_{n,l}\left(\rho\cos\theta,\rho\sin\theta,\rho\right)\cdot \\ \hat{\boldsymbol{\Omega}}_j(\rho\cos\theta,\rho\sin\theta)\rho d\rho d\theta. \end{aligned} \tag{8}$$

The output of this stage is the set of $(n+1)^2$ magnitudes of the pseudo-Zernike coefficients. From (4) the modulus of the pseudo-Zernike moments are rotational invariant. This means that at a given observation angle the modulus of the moments are independent of the relative orientation of the target in the image plane. Hence, the feature vector is

$$\boldsymbol{F} = \left[|\psi_{0,0}|, \ldots, |\psi_{N,-N}|\right]. \tag{9}$$

Finally, the feature vector, $\boldsymbol{F}$, is normalized using the following linear rescaling

$$\tilde{\boldsymbol{F}} = (\boldsymbol{F} - \mu_{\boldsymbol{F}})/\sigma_{\boldsymbol{F}}, \tag{10}$$

where $\mu_{\boldsymbol{F}}$ and $\sigma_{\boldsymbol{F}}$ are the mean and standard deviation of the feature vector. These values are then used to populate the features to be used as input to a classifier.

The last step of the algorithm consists of the classification procedure. The classification has been performed using a k-Nearest Neighbour (K-NN) classifier because of its low computational load and its capability of providing score values as an output [7], [8], however other classifiers with similar characteristics can also be selected.

The sum method is selected as fusion rule [7], [8] and is performed at the confidence level. Let V be the number of possible classes, for each of the J sensors, the k-NN classifier returns as output a V-dimensional vector $\mathbf{s}_j$ containing the confidence levels for each cluster. The confidence levels are defined as the number of nearest neighbours belonging to the v-th class divided by k. The sum of all the scores is then computed as

$$\boldsymbol{\lambda} = \sum_{j=1}^{J} \mathbf{s}_j, \tag{11}$$

with $\boldsymbol{\lambda} = [\lambda_1, \lambda_2, \ldots, \lambda_L]$, from which the estimated class can be selected

$$\hat{v} = \underset{v}{\operatorname{argmax}}\, \boldsymbol{\lambda}. \tag{12}$$

This fusion strategy allows the exploitation of the information from multiple images and is known for its robustness [7], [8] and allows the definition of the *unknown* class if a draw occurs, because $\boldsymbol{\lambda}$ could not have a unique maximum element, or if the maximum value of $\boldsymbol{\lambda}$ does not satisfy a specific requirement, such as a sufficient level of confidence.

III. Performance Analysis

In this section the performance analysis of the ATR algorithm described in Section II is presented. The algorithm is applied to real full polarimetric X-band SAR data. The dataset used in this analysis is the "Gotcha Volumetric SAR Data Set V1.0" [4], consisting of SAR phase history from a sensor with carrier frequency of 9.6 GHz and 640 MHz bandwidth, full azimuth coverage and 8 different elevation angles. The imaging scene consists of numerous civilian vehicles and calibration targets.

For our analysis the aperture has been divided in sub apertures of 4 degrees in azimuth in order to have approximately equal range-azimuth resolution cell of 23 cm. In this way 90 images (looks) for each of the 8 circular passes (different elevations) are available in four polarizations for each of the 9 commercial vehicles considered. In order to allow the reader to understand the imaged targets and scene, in Fig. 2 the 9 vehicles are shown; while in Fig. 3 the 360 degree full polarimetric image of the scene of interest is shown; the image is a multi-look image (including all the 90 looks of one circular pass). As already mentioned, for testing a single look is used. In Fig. 3, the 9 vehicles are labelled with alphabetic letters. Specifically, the 9 vehicles are: A) Chevrolet Prizm, B) Nissan Sentra, C) Nissan Maxima, D) CASE Tractor, E) Ford Taurus, F) Chevrolet Camry, G) Hyundai Santa Fe, H) Chevrolet Malibu, I) Hyster Forklift.

To perform the analysis equal sized sub-images (50×50 pixels) containing each vehicle are selected. Specifically, of the 8 available passes (different elevations) a subset of the pass with lower altitude is used to train the classifier while all the other images (i.e. the unused images from the lowest pass and all the images from the other seven, higher elevation, passes) are used to test the algorithm. Different elevation and azimuth angles are considered for testing the images to provide independent training and validation sets. Three

Fig. 2. Images of the 9 vehicles.

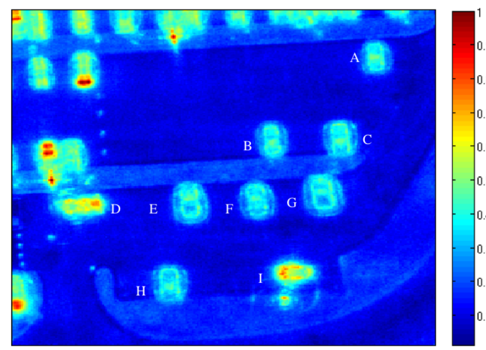

Fig. 3. Full Azimuth and full polarimetric magnitude SAR image of the area of interest containing the 9 vehicles.

analyses are presented, each of them performed with different selections of the training subset. The three training sets consist of 4, 10 and 30 images selected with azimuth spacing of of 92°, 36° and 12° respectively. The use of a limited number of aspect angles for training is meaningful in terms of a practical realization. Specifically the creation of the training database, and in terms of algorithm robustness with respect to classifying observations acquired from angles different from those used for training. The analysis is performed using 1, 2 and 3 test data images to characterize the benefits of the multi-sensor framework and the classification fusion stage. Moreover, to evaluate the performance of the classification algorithm, the correct classification, defined as the number of correctly classified sub-images over the total number of sub-images under test, is used as figure of merit. For the case of 1 test image all the available images have been used. For the case of 2 and 3 test images 10000 pairs or triples are chosen randomly. For this reason the standard deviation of the correct classification rate for the cases of 2 and 3 sensors is also computed.

In Fig. 4 examples of the tested configurations are shown. Multiple acquisitions can be assumed to be done by multiple platforms or from the same platform in different instants of time. Moreover the analysis is performed for different orders of the pseudo-Zernike moments between 1 and 20 and using a 3-NN classifier ($k = 3$). Fig. 5 shows the results obtained for 1, 2 and 3 platforms using a training samples spacing of 92°, equivalent to 4 observations of a target with different equally spaced initial azimuth angles (e.g. 0°, 92°, 184° and 276°). For the case of 2 and 3 platforms the $1 \times \sigma$ confidence intervals are less than 1%. From the results in Fig. 5 the algorithm shows a

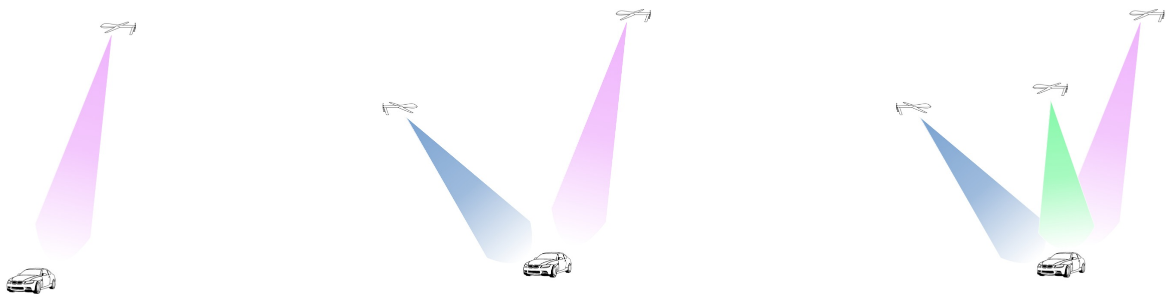

(a) 1 platform (b) 2 platforms (c) 3 platforms

Fig. 4. 1, 2 and 3 sensor acquisition examples.

good level of performance identifying the 9 different classes, despite the small amount of training observations available. The benefit of using multiple passes is evident and can be quantified in the order of 10% for both the 2 and 3 platforms cases. In addition the confidence intervals obtained with the 2 and 3 platform cases show that the performance result to be very stable. Table I shows an example of confusion matrix for the case of 1 Sensor, with an image spacing of $92°$, obtained with a pseudo-Zernike moments order equal to 10 (the corresponding correct classification is 56.23%). From Table I, it can be seen how the classification error occurs mainly for classes F, G and H, confused with classes C, B and C respectively.

Fig. 6 shows the results obtained with an angular spacing of $36°$. In this case a higher angular density of training samples allows the algorithm to perform better in all the analysed configurations, with the 3 platforms case approaching the 90% of correct identification.

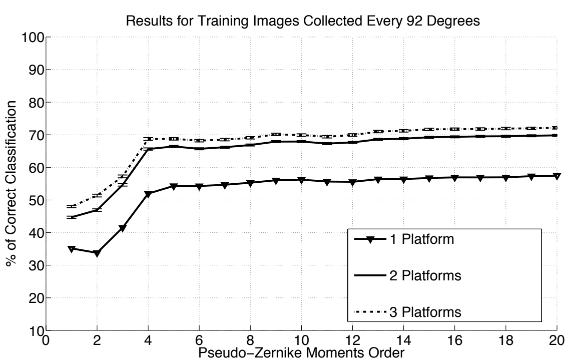

Fig. 5. Percentage of correct target classification vs order of the pseudo-Zernike moments obtained using 4 observations for training with spacing of $92°$.

For the results shown in Fig. 7 an angular of $12°$ was assumed, leading to 30 images used for training. This amount of training data corresponds to a third of all the possible observation angles. The algorithm performance increases for

TABLE I. CONFUSION MATRIX FOR THE 1 SENSOR CASE, IMAGE SPACING $92°$, PSEUDO-ZERNIKE MOMENTS ORDER 10.

class	A	B	C	D	E	F	G	H	I
A	582	17	3	0	23	0	0	3	88
B	11	590	7	16	10	52	25	1	4
C	4	43	605	0	29	17	0	18	0
D	2	80	7	425	202	0	0	0	0
E	7	118	16	106	465	4	0	0	0
F	10	131	360	12	24	175	1	2	1
G	5	423	19	54	63	60	79	0	13
H	0	15	594	2	56	15	0	34	0
I	38	9	0	0	0	0	0	0	669

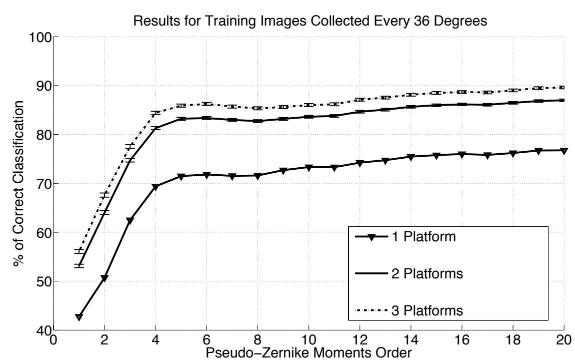

Fig. 6. Percentage of correct target classification vs order of the pseudo-Zernike moments obtained using 10 observations for training with spacing of $36°$.

the 1, 2 and 3 platforms case, with a maximum attained for the moment order 20, reaching, respectively, a correct classification of 92.43%, 96.85% and 98.26%.

Acquiring a training database with multiple observations per target represents a cost that is, in some cases, relatively time consuming (e.g. very high number of different classes to be populated). The second case considered ($36°$) represents a good trade-off between performance and costs.

Clearly, the proposed algorithm appears to have multiple advantages: reliable target identification, multi-observation fusion capabilities without the requirement of a multi-platform

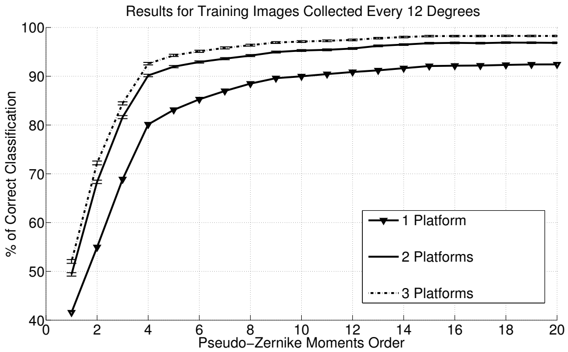

Fig. 7. Percentage of correct target classification vs order of the pseudo-Zernike moments obtained using 30 observations for training with spacing of $12°$.

training set, ability to provide good automatic target identification performances with a limited set of target observations as training, the capability to identify target observed from an angle different form those used for training. The pseudo-Zernike moments properties as translation and rotation independence makes the algorithm robust with respect to the relative target orientation in the image plane and not registered images between different platforms.

IV. Conclusion

In this paper a novel algorithm for automatic target recognition with the capability of target identification has been presented. The proposed algorithm exploits the pseudo-Zernike moments derived from full polarimetric SAR images as features used to identify different targets. Moreover, the algorithm allows the fusion of the classification result of each of multiple observations from different aspect angles. The classification capabilities of the proposed approach have been evaluated using real multiple passes full polarimetric SAR data of different commercial vehicles. The performances, in terms of correct target classification, have been quantified; moreover, the confusion matrix was used to identify cases in which the approach is less robust. The results have indicated a high confidence target identification and multi-observation fusion capabilities without the requirement of a multi-platform training set.

Acknowledgment

This work was supported by the Engineering and Physical Sciences Research Council (EPSRC) Grant number EP/K014307/1 and the MOD University Defence Research Collaboration in Signal Processing, University of Naples "Federico II" and Selex-ES.

References

[1] P. Tait, *Introduction to Radar Target Recognition*, IEE Radar Series. Institution of Engineering and Technology, 2005.

[2] L. M. Novak, G. R. Benitz, G. J. Owirka, and L. A. Bessette, "Atr performance using enhanced resolution sar," 1996, vol. 2757, pp. 332–337.

[3] L. M. Novak, G. J. Owirka, and W. S. Brower, "An efficient multi-target sar atr algorithm," in *Thirty-Second Asilomar Conference on Signals, Systems & Computers*, 1998, vol. 1, pp. 3–13.

[4] E. Ertin, C. D. Austin, S. Sharma, O. L. Moses, and L. C. Potter, "GOTCHA Experience Report: Three-Dimensional SAR Imaging with Complete Circular Apertures," in *SPIE Proceedings*, 2007, vol. 6568.

[5] A. B. Bhatia and E. Wolf, "On the Circle Polynomials of Zernike and Related Orthogonal Sets," *Mathematical Proceedings of the Cambridge Philosophical Society*, vol. 50, pp. 40–48, January 1954.

[6] L. Pallotta, C. Clemente, A. De Maio, J. Soraghan, and A. Farina, "Pseudo-Zernike Moments Based RadarMicro-Doppler Classification," in *IEEE Radar Conference, Cincinnati, USA*, 19-23 May 2014.

[7] R.O. Duda, P.E. Hart, and D.G. Stork, *Pattern classification*, Pattern Classification and Scene Analysis: Pattern Classification. Wiley, 2001.

[8] K. Fukunaga, *Introduction to Statistical Pattern Recognition*, Computer Science and Scientific Computing. Elsevier Science, 1990.